

The Gamma-Ray-Flux Probability Distribution Function from Galactic Halo Substructure

Samuel K. Lee, Shin'ichiro Ando, and Marc Kamionkowski
California Institute of Technology, Mail Code 130-33, Pasadena, CA 91125
 (Dated: November 11, 2019)

One of the targets of the recently launched Fermi Gamma-ray Space Telescope is a diffuse gamma-ray background from dark-matter annihilation or decay in the Galactic halo. N-body simulations and theoretical arguments suggest that the dark matter in the Galactic halo may be clumped into substructure, rather than smoothly distributed. Here we propose the gamma-ray-flux probability distribution function (PDF) as a probe of substructure in the Galactic halo. We calculate this PDF for a phenomenological model of halo substructure and determine the regions of the substructure parameter space in which the PDF may be distinguished from the PDF for a smooth distribution of dark matter. The PDF allows a statistical detection of substructure, even if individual halos cannot be detected. It may also allow detection of substructure on the smallest microhalo mass scales, $\sim M_\oplus$, for weakly-interacting massive particles. Furthermore, it provides a method to measure the substructure mass function.

PACS numbers: 95.85.Pw, 95.35.+d, 98.35.Gi

I. INTRODUCTION

It has long been a goal of astrophysics and cosmology to determine the distribution and nature of the dark matter that populates our Galactic halo. Only more recently have we begun to focus on the possibility to detect substructures in the Galactic halo [1]. In hierarchical structure formation, small gravitationally bound dark-matter systems form first and then merge to form progressively more massive systems. In each stage, some of the earlier generations of structure may remain intact after merging, and so the Milky Way halo may contain substructures over a wide array of masses. Scaling arguments suggest that substructures may continue all the way down to the smallest mass scales at which there is primordial power [2], although the precise details may be uncertain [3]. If weakly-interacting massive particles (WIMPs) [4] make up the dark matter, the cutoff mass should be in the range $10^{-6} - 10^2 M_\oplus$ [5], and if axions [6] make up the dark matter, it may be as small as $10^{-12} M_\oplus$ [7].

If WIMPs make up the dark matter, there may be several avenues toward detecting them. With the launch of the Fermi Gamma-ray Space Telescope (formerly GLAST) [8], however, there is now particular attention being paid to detection of energetic gamma rays from dark-matter annihilation in the Galactic halo (see, e.g., Ref. [9] and references therein). While the diffuse flux from such annihilations have been considered for a long time [10], the possibility to detect substructure, through angular variations in the background, is more recent [11, 12, 13]. It is possible that individual substructures may be resolved [14]. Proper motions of the smallest microhalos have also been considered [15].

In this paper, we propose the one-point gamma-ray-flux probability distribution function (PDF) as a probe of halo substructure. If dark matter is smoothly distributed, then the variation in the number of diffuse-background photons from one pixel to another should

arise only from Poisson fluctuations. If, however, there is substructure, there will be additional flux variations from pixel to pixel. This may provide another route—an alternative to the angular two-point correlation function [11, 13]—to detect substructure statistically, especially for the very smallest microhalo mass scales.¹ It may also allow measurement of the substructure mass function.

We illustrate with a phenomenological model for Galactic substructure in which a fraction f of the halo is made of dark-matter microhalos with a power-law mass function (with a lower mass cutoff M_{\min}) and a constant mass-to-gamma-ray-luminosity ratio $\Upsilon = M_{\min}/L_{\min}$. The next Section introduces this model and discusses the constraints from the Energetic Gamma Ray Experiment Telescope (EGRET) [17] to the parameter space. In Section III, we calculate the flux PDF for this model and discuss the translation to a discrete distribution of counts in each Fermi pixel. We provide in Section IV numerical results for the PDF for an illustrative model. Section V determines the regions of the $L_{\min}-(M_{\min}/f)$ parameter space in which the PDF of substructure can be distinguished from that of a smoothly distributed background. In Section VI we summarize and comment on additional steps that must be taken to implement this probe.

II. MICROHALO MODEL AND EGRET CONSTRAINTS

We assume that a fraction f of the dark matter in the Galactic halo is composed of objects with a power-law mass function $dn_h/dM_h \propto M_h^{-\alpha}$, independent of Galactocentric radius r . We shall take $\alpha = 2$ in this work

¹ It has been similarly suggested [16] that background fluctuations may be used to learn about the traditional astrophysical sources contributing to the diffuse background.

when evaluating numerical results, but our approach will hold in general. Normalization of the mass function is obtained by the relation,

$$f\rho(r) = \int_{M_{\min}}^{M_{\max}} dM_h M_h \frac{dn_h}{dM_h}(r, M_h) \equiv \langle M_h \rangle n_h(r), \quad (1)$$

where $\rho(r)$ is the density profile of the Milky Way halo, M_{\min} and M_{\max} are the masses of the smallest and largest subhalos, and in the last equality we define the mean mass $\langle M_h \rangle$ as well as spatial number density $n_h(r)$ of microhalos. From Eq. (1) and the assumed shape of the mass function, we obtain

$$\frac{dn_h}{dM_h}(r, M_h) = \frac{f\rho(r)}{\ln(M_{\max}/M_{\min})} M_h^{-2}, \quad (2)$$

$$n_h(r) = \frac{f\rho(r)}{M_{\min} \ln(M_{\max}/M_{\min})}, \quad (3)$$

$$\langle M_h \rangle = M_{\min} \ln(M_{\max}/M_{\min}), \quad (4)$$

where in Eq. (3), we assumed $M_{\min} \ll M_{\max}$. We use the NFW [18] profile,

$$\rho(r) = \frac{\rho_s}{(r/r_s)(1+r/r_s)^2}, \quad (5)$$

where $\rho_s = 5.4 \times 10^{-3} M_{\odot} \text{ pc}^{-3}$ is the characteristic density, and $r_s = 21.7 \text{ kpc}$ is the scale radius. The density is set to zero beyond a cutoff radius $r_c = 10 r_s$. This normalizes the mass of the Milky Way halo to be $10^{12} M_{\odot}$, and gives $\rho_0 = 7 \times 10^{-3} M_{\odot} \text{ pc}^{-3}$ as the local density at the solar radius ($r_0 = 8.5 \text{ kpc}$).

We assume that the gamma-ray luminosity L_h of each microhalo is proportional to its mass, with constant mass-to-light ratio $\Upsilon \equiv M_h/L_h$. Then, the luminosity function is $dn/dL_h = \Upsilon(dn/dM_h)$. Note that throughout this paper, the luminosity is the *number* (not energy) of photons emitted per unit time; similarly, we deal with number fluxes (fluences) and intensities. For clarity of presentation, we assume that the gamma rays are monoenergetic, with energy E , although the analysis applies equally well to a broader energy distribution.

The gamma-ray intensity $I(\psi)$ (units of photons $\text{cm}^{-2} \text{ sec}^{-1} \text{ sr}^{-1}$) from microhalos along a line of sight at an angular separation ψ from the Galactic center is

$$\begin{aligned} I(\psi) &= \frac{1}{4\pi} \int dl \int_{L_{\min}}^{L_{\max}} dL_h L_h \frac{dn_h}{dL_h}(r(l, \psi), L_h) \\ &= \frac{f}{4\pi\Upsilon} \int dl \rho(r(l, \psi)), \end{aligned} \quad (6)$$

where l is the distance along the line of sight; i.e., $r^2 = r_0^2 + l^2 - 2r_0 l \cos \psi$. We plot in Fig. 1 the intensity $I_6 \equiv I/(10^{-6} \text{ cm}^{-2} \text{ sec}^{-1} \text{ sr}^{-1})$, as a function of direction ψ , for the fiducial values $f\Upsilon^{-1} = 10^{30} M_{\odot}^{-1} \text{ sec}^{-1}$; the result scales with $f\Upsilon^{-1}$.² We also plot (with arbitrary nor-

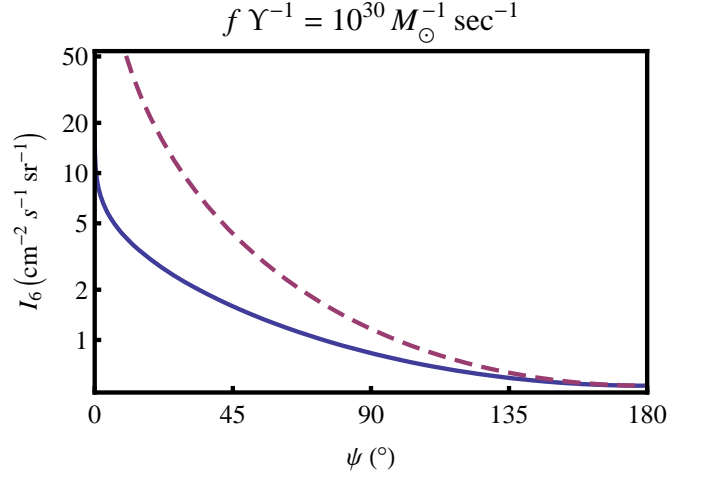


FIG. 1: The intensity $I(\psi)$ from microhalos as a function of the angle ψ the line of sight makes with the Galactic center (solid) for fiducial values of the parameters M_h , L_h , and f . We also plot (dashed) the angular variation of the intensity from dark-matter annihilation of a smooth component, normalized to match the intensity from the microhalo component at Galactic anti-center. Note that the variation with ψ of the gamma-ray flux from substructure is not as dramatic as that from annihilation in a smooth component.

malization) the angular dependence of the intensity from dark-matter annihilation from a smooth halo in order to show that it varies more rapidly with ψ than the angular dependence of the gamma-ray intensity from substructure.

The current upper bound to the diffuse gamma-ray background from EGRET places an upper limit to $f\Upsilon^{-1}$. We approximate the upper limit from Ref. [19] to the gamma-ray intensity, averaged over the $10^\circ \times 10^\circ$ region around the Galactic center, by $2 \times 10^{-6} (E/\text{GeV})^{-1/2} \text{ cm}^{-2} \text{ sec}^{-1} \text{ sr}^{-1}$ over the energy range $0.1 \text{ GeV} < E < 10 \text{ GeV}$ (see also Ref. [20]), and we then derive an upper limit,

$$\frac{f}{\Upsilon} \lesssim 3 \times 10^{29} (E/\text{GeV})^{-1/2} M_{\odot}^{-1} \text{ sec}^{-1}. \quad (7)$$

III. CALCULATION OF THE PDF

The Fermi angular resolution is roughly 0.1° ; throughout this paper we shall assume square pixels of solid angle $(0.1^\circ)^2$. This implies that the background flux will be measured in $\sim 4 \times 10^6$ beams on the sky. One can then make a histogram of the number of counts in each beam.

at $\psi = 0$. However, the flux from any finite-size window about the Galactic center involves an integral over the intensity, and the divergence of $I(\psi)$ at $\psi = 0$ is such that the flux is always finite.

² Note that if $\rho(r) \propto r^{-1}$ as $r \rightarrow 0$, the intensity is formally infinite

Our goal here is to make predictions for the shape $P(F)$ for the distribution of these fluxes, under the assumption that these photons come from dark-matter annihilation in a clumpy Galactic halo.

Although $P(F)$ will in general be a function of the line-of-sight direction ψ , we shall suppress this dependence in much of the presentation, reinserting it later when required for numerical results. We also refer to all probability distribution functions as $P(x)$; the particular function under discussion should be clear from the argument x .

If the population of sources has a flux-density distribution $P_1(F)$, then the probability $P(F)$ to see a total flux F (integrated over all sources in the beam) in a given beam is [21]

$$P(F) = \mathcal{F}^{-1} \left\{ e^{\mu(\mathcal{F}\{P_1(F)\}-1)} \right\}. \quad (8)$$

Here $\mathcal{F}\{x\}$ is the Fourier transform of x and \mathcal{F}^{-1} its inverse, and the flux-density distribution $P_1(F)$ is normalized to $\int P_1(F) dF = 1$. The quantity

$$\mu(\psi) = \frac{\Omega_{\text{beam}} f}{\langle M_h \rangle} \int_0^{l_c(\psi)} l'^2 \rho(r(l', \psi)) dl', \quad (9)$$

is the mean number of sources in each beam of solid angle Ω_{beam} (in sr). We reproduce in the Appendix the derivation of Eq. (8) originally provided by Ref. [21].

A. Derivation of $P_1(F)$

The first step is thus to find the flux-density distribution $P_1(F)$ for individual sources in the beam. This depends on the luminosity function and on the spatial distribution of microhalos. The luminosity function is $P(L_h) \propto L_h^{-\alpha}$, where again we take $\alpha = 2$. The probability for an individual microhalo to be at a distance l along a line of sight ψ is $P(l, \psi) \propto l^2 \rho(r(l, \psi))$. We take a maximum cutoff at $l_c(\psi)$, corresponding to a cutoff radius $r_c = r(l_c(\psi), \psi)$.

We then find $P_1(F)$ is given by

$$\begin{aligned} P_1(F, \psi) &= \int dl dL_h P(l, \psi) P(L_h) \delta \left(F - \frac{L_h}{4\pi l^2} \right) \\ &\propto \int_0^{l_c(\psi)} dl l^4 \rho(r(l, \psi)) (l^2 F)^{-\alpha} \\ &\quad \times \theta(4\pi l^2 F - L_{\min}) \theta(L_{\max} - 4\pi l^2 F) \\ &\propto F^{-\alpha} \int_{l(L_{\min}, F)}^{\min[l_c(\psi), l(L_{\max}, F)]} dl l^{4-2\alpha} \rho(r(l, \psi)), \end{aligned} \quad (10)$$

where the step functions enforce the cutoffs in $P(L_h)$, and $l(L_i, F) \equiv (L_i/4\pi F)^{1/2}$. Note also the implicit cutoff in $P_1(F)$ for $F < L_{\min}/4\pi l_c^2$. Eq. (10) can be evaluated numerically for a given value of the parameter L_{\min} ; the result is presented in Fig. 2 for a fiducial value of L_{\min} .

Note that Eq. (10) yields the familiar $P_1(F) \propto F^{-5/2}$ (conventionally written as $N(> S) \propto S^{-3/2}$) for a homogeneous spatial distribution of sources with a general luminosity function, if the condition $l_c(\psi) \geq l(L_{\max}, F)$ is satisfied over the range of F of interest. Under this condition, $P_1(F)$ will also asymptote to $F^{-5/2}$ at large F for a non-pathological spatial distribution. However, if $l_c(\psi) < l(L_{\max}, F)$ for values of F within the range of interest, then there will be a break in $P_1(F)$; $P_1(F)$ will tend to $F^{-\alpha}$ at F for which the second condition holds, and will then tend to $F^{-5/2}$ at higher F .

For the problem under discussion, values of L_{\max} in the interesting regions of parameter space are such that $P_1(F)$ is negligible in the $F^{-5/2}$ regime. Thus, the essential “large- F ” dependence of $P_1(F)$ will be $F^{-\alpha}$.

B. Calculation of the Counts Distribution

Since the photon counts from Fermi will be very low, we will need to discretize the continuous variable F . We will observe F in terms of photons $\text{beam}^{-1} \text{ year}^{-1}$, or similar units. Furthermore, emission of photons is a Poisson process. Thus, let the number of photons measured in a given beam over an observation period T be $C \approx EF \in \mathbb{N}$; here E is the exposure in a beam given in units of $\text{cm}^2 \text{ sec}$, and is given by $E \approx AT$, where $A \approx 2000 \text{ cm}^2$ is the area of the detector. We take $T = 1 \text{ year}$ in this paper. The discrete probability distribution

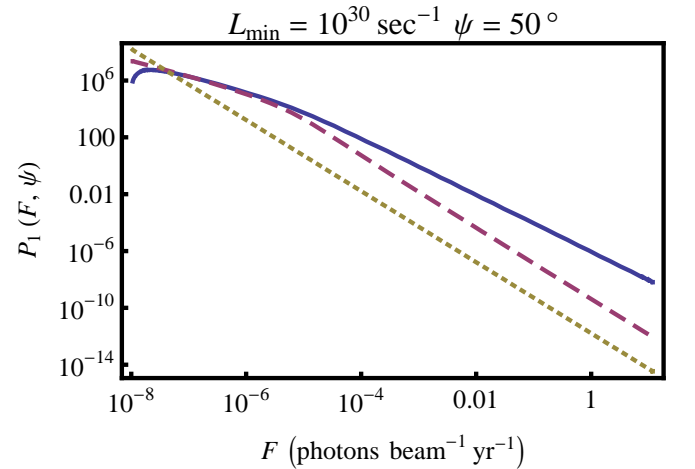


FIG. 2: The flux-density distribution $P_1(F, \psi = 50^\circ)$ for the flux from an individual microhalo drawn from a population of microhalos with: (1) an NFW spatial distribution and a luminosity function $\propto L_h^{-2}$, for a fiducial value of the minimum cutoff luminosity L_{\min} (solid); (2) an NFW spatial distribution and uniform luminosity L_{\min} (dashed); and (3) a homogeneous spatial distribution and uniform luminosity L_{\min} (dotted). Note that the first distribution tends to $P_1(F) \propto F^{-2}$ at large F , while the last two distributions tend to $P_1(F) \propto F^{-5/2}$. The break in the first distribution to an $F^{-5/2}$ dependence occurs at an F above the range displayed.

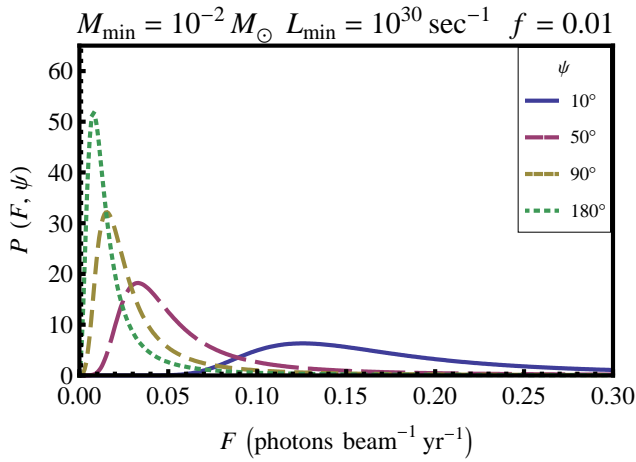


FIG. 3: The continuous probability distribution function $P(F, \psi)$ for the total number flux F in a given beam along a line of sight at an angle ψ from the Galactic center, for fiducial values of the parameters M_{\min} , L_{\min} , and f and various values of ψ .

bution $P(C)$ is then given by the sum of Poisson distributions with mean EF weighted by $P(F)$:

$$P(C) = \int_0^\infty P(F) \wp(EF, C) dF, \quad C \in \mathbb{N}. \quad (11)$$

The shape of the discrete distribution $P(C)$ is generally very similar to that of the continuous distribution $P(EF)$ and is only slightly modified at the low end. Note that Eq. (11) is easily modified to include a diffuse background or a smooth dark-matter halo; the flux from these components can simply be added to the mean of the Poisson distribution in the integrand.

IV. NUMERICAL RESULTS

Fig. 3 shows the results of numerical tabulation of the PDF $P(F)$ for a set of fiducial model parameters. These parameters predict a mean intensity consistent with, but near the upper limit to, the current EGRET upper bound. The PDF has a peak at low F and a power-law tail at high F .

If the mass-to-light ratio Υ is increased, with M_{\min} and f held fixed (equivalently, if L_{\min} is decreased), then the photon flux decreases. The entire distribution is then scaled down along the F -axis, and the peaks in Fig. 3 are shifted to the left. If M_{\min} is reduced, with Υ and f held fixed, then the relative widths of the peaks decrease. This behavior can be understood by considering the limit $M_{\min} \rightarrow 0$; in this case, we should expect to recover a smooth spatial distribution, resulting in a delta-function $P(F)$.

The distribution $P(C)$ for discretized counts C is plotted in Fig. 4, for a one-year Fermi exposure. Also plotted

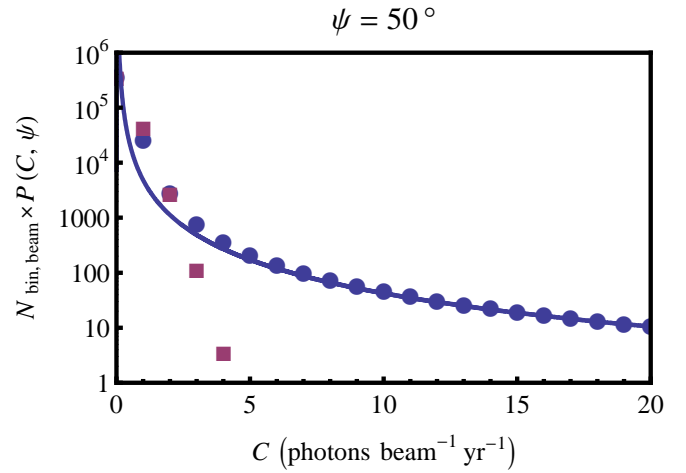


FIG. 4: The discrete probability distribution function $P(C, \psi = 50^\circ)$ for the total number flux C in a given beam along a line of sight at an angle ψ from the Galactic center (circles), for fiducial parameter values (identical to those used in Figure 3). The continuous $P(F, \psi = 50^\circ)$ (solid) and a fitted Poisson distribution (squares) are also plotted for comparison. We have normalized to $N_{\text{beam, bin}} = N_{\text{beam}}/10$ (assuming that this is a representative size of the bins in ψ), where $N_{\text{beam}} = 4\pi/(0.1^\circ)^2 \approx 4 \times 10^6$ is the number of beams at the angular resolution limit. The Poisson errors are comparable to the size of the points.

is the Poisson distribution for a smoothly distributed diffuse background of the same mean flux. As the Figure indicates, the large- F power-law tail of the PDF is qualitatively different than the exponential falloff of the Poisson distribution with F . Thus, detection of substructure amounts to detection of such a power-law tail.

Furthermore, the power-law tail of $P(F)$ follows the power-law tail of $P_1(F)$. This is simply because single bright sources dominate beams with high F . However, as discussed in Subsection III A, the power-law tail of $P_1(F)$ in turn follows the power-law of the mass function. For example, the power-law tail in Fig. 4 indeed follows an F^{-2} dependence. Thus, $P(F)$ not only provides a method of substructure detection; it can also reveal the substructure mass function.

V. DETECTABILITY

Fig. 4 is plotted for a model in which the mean flux is comparable to the EGRET upper limit. Fermi, however, should be sensitive to much lower-level fluxes. If the mean flux is lower than the values assumed in Fig. 4, then the amplitude of the power-law tail in Fig. 4 will be reduced. It will thus be harder to detect. In this Section, we determine the regions of the model parameter space in which the PDF can be distinguished from the Poisson distribution expected for a smooth or diffuse background of the same mean flux.

We determine the signal-to-noise with which the PDF

$P(C)$ can be distinguished from the Poisson distribution $\wp(\langle C \rangle, C)$ with the same mean count rate $\langle C \rangle$. The null hypothesis of no substructure can be eliminated at the 3σ level if $S/N > 3$, where

$$\frac{S}{N} = \sqrt{\sum_{\psi_i} N_{\text{beam}, \text{bin}}(\psi_i) \left(\frac{S}{N}\right)_{\psi_i}^2}, \quad (12)$$

and

$$\left(\frac{S}{N}\right)_{\psi_i}^2 = \sum_{C=0}^{C_{\text{max}}(\psi_i)} \frac{[P(C, \psi_i) - \wp(\langle C \rangle_{\psi_i}, C)]^2}{\wp(\langle C \rangle_{\psi_i}, C)}. \quad (13)$$

Here, we label the angular bins by the central value of the bin ψ_i . The quantity $N_{\text{beam}, \text{bin}}(\psi_i)$ is the number of beams contained in each bin, and $C_{\text{max}}(\psi_i)$ is the highest count observed in each bin, and $\langle C \rangle_{\psi_i}$ is the mean of the best-fit Poisson distribution in each bin. Eq. (12) then quantifies the difference between the discrete probability distributions $P(C, \psi)$ and $\wp(\langle C \rangle_{\psi}, C)$, comparing the substructure PDF with the Poissonian distribution expected from a non-isotropic diffuse background. In Fig. 5, we plot the regions of the $L_{\text{min}}-(M_{\text{min}}/f)$ parameter space in which the value of S/N indicates that substructure can be detected. Also plotted are the regions of the parameter space ruled out already by the current EGRET upper limit to the diffuse background.

Our particular definition of S/N tests the PDF against the null hypothesis of a non-isotropic diffuse background; it gives $S/N = 0$ if the null hypothesis is true, and a large S/N if the null hypothesis is to be rejected. However, the position of the line in Fig. 5 indicating the Poissonian region of parameter space is essentially independent of the definition of S/N . To see this, let us examine low-mean-flux models. It is clear that we cannot distinguish $P(C)$ for a given model from a general Poissonian distribution if $N_{\text{beam}} \times P(C) < 1$ for all $C \geq 2$ (i.e., if the mean flux is so low that all observed counts are at most one photon, and we observe no pixels receiving two or more photons). This then implies that the $P(C)$ of a low-mean-flux model, with $N_{\text{beam}} \times P(C) < 1$ for all $C > 2$, must at least satisfy $N_{\text{beam}} \times P(C=2) \geq 1$ to be distinguishable from a Poisson distribution. This is then the condition for minimally-detectable substructure, and essentially defines the Poissonian region of parameter space independently of the particular definition of S/N . To see this, note that since $\langle C \rangle$ is extremely small for low-mean-flux models, $N_{\text{beam}} \times \wp(\langle C \rangle, C=2) \ll 1$. It follows that alternate definitions of S/N would also give large values of S/N in the case of minimally-detectable substructure, provided that they test against the null hypothesis of a Poissonian distribution.

Note that in Fig. 5 we have neglected the flux from the diffuse background and the smooth dark-matter component. If we include these additional backgrounds in our model, then we find a stronger constraint on high-mean-flux microhalo models. This is simply because the combined mean flux of the microhalos and the backgrounds

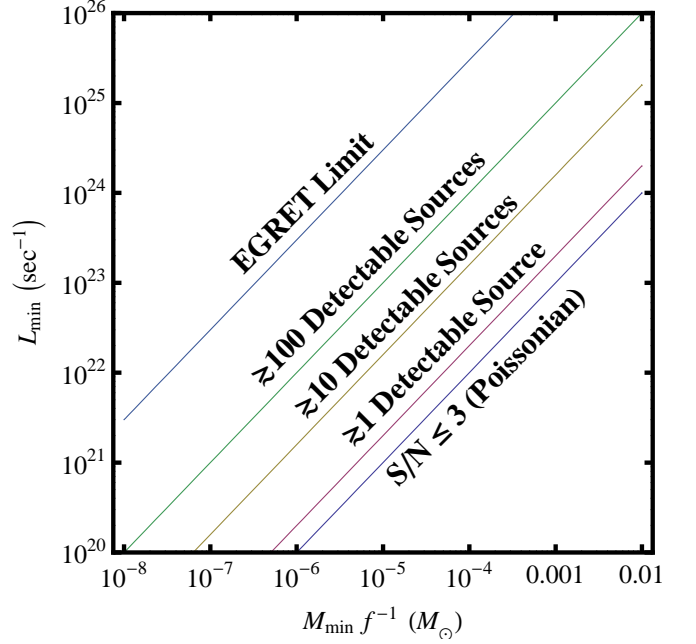


FIG. 5: The $L_{\text{min}}-(M_{\text{min}}/f)$ parameter space. We indicate the region that is already ruled out by the EGRET upper limit to the diffuse background; where there will be $\gtrsim 1$, $\gtrsim 10$, and $\gtrsim 100$ detectable point sources with $F \geq 3$ photons $\text{beam}^{-1} \text{ year}^{-1}$; and where measurements of the flux PDF cannot be distinguished from a Poissonian distribution. Angular bins with widths of $\Delta\psi = 30^\circ$ were used in the calculation of S/N .

cannot exceed the EGRET limit. Also, the power-law tails of low-mean-flux models may be dominated by additional backgrounds, effectively increasing the size of the Poissonian regime. Including backgrounds in the model thus increases the regions of $L_{\text{min}}-(M_{\text{min}}/f)$ parameter space that can be ruled out via observation of substructure, ultimately providing stronger constraints on the parameters in the case of positive detection.

Of course, detection of a nontrivial PDF is also intimately related to the criteria for detection of point sources. The number of sources observed with flux greater than F is given by

$$N(\geq F) = \frac{2\pi f}{\langle M_h \rangle} \int d\psi \sin \psi \int dL_h P(L_h) \times \int_0^{l(L_h, F)} l^2 \rho(r(l, \psi)) dl. \quad (14)$$

In certain regions of the parameter space for which Fig. 5 indicates a nontrivial PDF, substructure will be detectable via detection of individual microhalos, even without a detailed analysis of the PDF. We plot these regions, taking the Fermi point-source-detection criterion of ≥ 3 photons per beam. The advantage of the full PDF, however, is that substructure can be detected even in regions of parameter space where individual microhalos elude detection. Measurement of the detailed shape

of the PDF can also provide more information on the microhalo mass function and/or spatial distribution in the halo than would be obtained simply by point-source counts.

VI. CONCLUSIONS AND COMMENTS

Here we have proposed that the distribution of fluxes measured in individual Fermi pixels can be used to probe the existence of substructure in the Galactic halo to very small mass scales. By characterizing fluctuations in the diffuse gamma-ray background in this way, the existence of Galactic substructure may be inferred statistically even if individual halos cannot be detected. This statistical approach should be viewed as complementary to the use of an angular correlation function [11, 13]. Since the PDF is a convolution of the microhalo mass function and spatial distribution, constraints to the parameters of these distributions may be obtained by measuring the PDF.

The full PDF we have calculated may be useful even in situations where individual microhalos can be detected. For example, the flux in a pixel with a 3σ excess which is interpreted as detection of a single point source may actually be due to several point sources; the probability that this is so may be inferred from the PDF.

We have illustrated the PDF that results in a phenomenological model for substructure parameterized by a fraction f of halo mass in substructure, a microhalo mass cutoff M_{\min} , and a mass-to-light ratio Υ . This is almost certainly an oversimplification. In more realistic models, the mass function may differ from the particular power law we have assumed. The mass-to-light ratio may depend on the microhalo mass, and there may even be a spread of luminosities for each mass. There may be a contribution to the background from a smoothly distributed component of dark matter. We have also assumed here that each microhalo will fall within a single resolution element of Fermi. Taking into account the finite angular size of each microhalo will reduce the length of the power-law tails in the PDF. However, this should be a relatively small correction for the smaller microhalo masses most important here. Similarly, contributions to the PDF from astrophysical backgrounds (e.g., from cosmic-ray spallation) may need to be considered before a complete comparison of our model predictions with data can be made. We leave the inclusion of these additional levels of complication to future work.

In addition to these future directions, one may also consider going further by combining the angular-correlation and PDF approaches. For example, the full two-point flux probability distribution function can be calculated and may provide additional observables with which to constrain the models or to distinguish a dark-matter background from other astrophysical backgrounds. Again, this is left for future investigation.

Acknowledgments

This work was supported by the Sherman Fairchild Foundation (SA), DoE DE-FG03-92-ER40701, and the Gordon and Betty Moore Foundation.

Appendix: Derivation of $P(F)$

Here we derive the relation between the flux-density distribution $P_1(F)$ and the flux PDF $P(F)$. Such a calculation is termed “ $P(D)$ analysis” in the literature, as it was first performed for observations of faint radio sources that produced “deflections” of the measuring apparatus [21]. This $P(D)$ analysis is useful in determining if an observed diffuse background is actually composed of numerous faint point sources. If this is the case, then there will be fluctuations in the diffuse signal from the random Poisson clustering of point sources in each beam. The shape of $P(F)$ thus depends not only on $P_1(F)$, but also the mean number μ of sources [Eq. (9)] in each beam.

We wish to find the probability distribution for a total flux F in a beam, given that it is the sum $F = \sum_i^k F_i$ of the fluxes F_i from individual microhalos. Each of the F_i is a random variable with probability distribution $P_1(F_i)$. Furthermore, the number k of fluxes F_i entering into the sum is itself a random variable given by a Poisson distribution with mean μ . Let us call $P_k(F)$ the probability that k random variables F_i sum to F ; i.e., the probability that k microhalos emit a total flux F . Then

$$P(F) = \sum_{k=0}^{\infty} \wp(\mu, k) P_k(F), \quad (15)$$

where $\wp(\mu, k)$ is a Poisson probability distribution for k with mean μ .

It now remains to determine $P_k(F)$. For $k = 0$, it is clear that $P_0(F) = \delta(F)$; $P_1(F)$ is given. For $k > 1$, $P_k(F)$ is given by

$$P_k(F) = \int_0^{\infty} dF_1 \dots \int_0^{\infty} dF_k \left(\prod_{i=1}^k P_1(F_i) \right) \delta(F - \sum_{i=1}^k F_i). \quad (16)$$

The easiest way to compute Eq. (16) is to note that the Dirac delta function transforms the integral into a convolution [16, 21]. To see this, let us examine the integral for $k = 2$:

$$\begin{aligned} P_2(F) &= \int_0^{\infty} dF_1 \int_0^{\infty} dF_2 P_1(F_1) P_1(F_2) \delta(F - (F_1 + F_2)) \\ &= \int_0^{\infty} dF_1 P_1(F_1) P_1(F - F_1) \\ &= (P_1 * P_1)(F). \end{aligned}$$

It follows that $P_k(F) = (P_{k-1} * P_1)(F)$; then by induction, $P_k(F)$ is given by $P_1(F)$ convolved (or autocorrelated) with itself k times. Using the convolution theorem,

it then follows that

$$P_k(F) = \mathcal{F}^{-1} \left\{ \mathcal{F} \{ P_1(F) \}^k \right\}, \quad (17)$$

where \mathcal{F} denotes a Fourier transform. Note that Eq. (17) also holds for $k = 0$ (and trivially for $k = 1$).

Inserting Eq. (17) into Eq. (15) and using the linearity of the inverse Fourier transform, we find

$$\begin{aligned} P(F) &= \sum_{k=0}^{\infty} \frac{e^{-\mu} \mu^k}{k!} \mathcal{F}^{-1} \left\{ \mathcal{F} \{ P_1(F) \}^k \right\} \\ &= e^{-\mu} \mathcal{F}^{-1} \left\{ \sum_{k=0}^{\infty} \frac{(\mu \mathcal{F} \{ P_1(F) \})^k}{k!} \right\} \\ &= \mathcal{F}^{-1} \left\{ e^{\mu (\mathcal{F} \{ P_1(F) \} - 1)} \right\}. \end{aligned} \quad (18)$$

Eq. (18) gives the desired relation for $P(F)$ in terms of $P_1(F)$ and μ . Although the presence of the inverse Fourier transform prevents further analytic simplification in general, this expression can be computed numerically using fast Fourier transforms on a discretized $P_1(F)$.

-
- [1] S. Ghigna, B. Moore, F. Governato, G. Lake, T. Quinn and J. Stadel, *Mon. Not. Roy. Astron. Soc.* **300**, 146 (1998) [arXiv:astro-ph/9801192]; A. A. Klypin, A. V. Kravtsov, O. Valenzuela and F. Prada, *Astrophys. J.* **522**, 82 (1999) [arXiv:astro-ph/9901240]; A. A. Klypin, S. Gottlöber, A. V. Kravtsov and A. M. Khokhlov, *Astrophys. J.* **516**, 530 (1999); B. Moore, S. Ghigna, F. Governato, G. Lake, T. Quinn, J. Stadel and P. Tozzi, *Astrophys. J.* **524**, L19 (1999); V. Berezinsky, V. Dokuchaev and Y. Eroshenko, arXiv:0712.3499 [astro-ph]; A. Loeb and M. Zaldarriaga, *Phys. Rev. D* **71**, 103520 (2005) [arXiv:astro-ph/0504112]; E. Bertschinger, *Phys. Rev. D* **74**, 063509 (2006) [arXiv:astro-ph/0607319]; J. Diemand, M. Kuhlen and P. Madau, *Astrophys. J.* **667**, 859 (2007) [arXiv:astro-ph/0703337]; C. Giocoli, L. Pieri and G. Tormen, arXiv:0712.1476 [astro-ph]; A. Helmi, S. D. M. White and V. Springel, *Phys. Rev. D* **66**, 063502 (2002) [arXiv:astro-ph/0201289]; D. Reed, F. Governato, T. Quinn, J. Gardner, J. Stadel and G. Lake, *Mon. Not. Roy. Astron. Soc.* **359**, 1537 (2005) [arXiv:astro-ph/0406034]; V. Springel *et al.*, arXiv:0809.0898 [astro-ph].
- [2] A. M. Green, S. Hofmann and D. J. Schwarz, *Mon. Not. Roy. Astron. Soc.* **353**, L23 (2004) [arXiv:astro-ph/0309621]; A. M. Green, S. Hofmann and D. J. Schwarz, *AIP Conf. Proc.* **805**, 431 (2006) [arXiv:astro-ph/0508553]; A. M. Green, S. Hofmann and D. J. Schwarz, *JCAP* **0508**, 003 (2005) [arXiv:astro-ph/0503387]; J. Diemand, M. Kuhlen and P. Madau, *Astrophys. J.* **649**, 1 (2006) [arXiv:astro-ph/0603250]; J. Diemand, B. Moore, and J. Stadel, *Nature* **433**, 389 (2005) [arXiv:astro-ph/0501589]; M. Kamionkowski and S. M. Koushiappas, *Phys. Rev. D* **77**, 103509 (2008) [arXiv:0801.3269 [astro-ph]].
- [3] H. Zhao, J. E. Taylor, J. Silk and D. Hooper, *Astrophys. J.* **654**, 697 (2007) [arXiv:astro-ph/0508215]; H. S. Zhao, J. Taylor, J. Silk and D. Hooper, arXiv:astro-ph/0502049; T. Goerdt, O. Y. Gnedin, B. Moore, J. Diemand and J. Stadel, *Mon. Not. Roy. Astron. Soc.* **375**, 191 (2007) [arXiv:astro-ph/0608495]; V. Berezinsky, V. Dokuchaev and Y. Eroshenko, *Phys. Rev. D* **73**, 063504 (2006) [arXiv:astro-ph/0511494].
- [4] G. Jungman, M. Kamionkowski and K. Griest, *Phys. Rept.* **267**, 195 (1996) [arXiv:hep-ph/9506380]; G. Bertone, D. Hooper and J. Silk, *Phys. Rept.* **405**, 279 (2005) [arXiv:hep-ph/0404175]; D. Hooper and S. Profumo, *Phys. Rept.* **453**, 29 (2007) [arXiv:hep-ph/0701197].
- [5] X. l. Chen, M. Kamionkowski and X. m. Zhang, *Phys. Rev. D* **64**, 021302 (2001) [arXiv:astro-ph/0103452]; S. Profumo, K. Sigurdson and M. Kamionkowski, *Phys. Rev. Lett.* **97**, 031301 (2006) [arXiv:astro-ph/0603373].
- [6] M. S. Turner, *Phys. Rept.* **197**, 67 (1990); G. G. Raffelt, *Phys. Rept.* **198**, 1 (1990); L. J. Rosenberg and K. A. van Bibber, *Phys. Rept.* **325**, 1 (2000); S. J. Asztalos, L. J. Rosenberg, K. van Bibber, P. Sikivie and K. Zioutas, *Ann. Rev. Nucl. Part. Sci.* **56**, 293 (2006).
- [7] M. C. Johnson and M. Kamionkowski, arXiv:0805.1748 [astro-ph].
- [8] glast.gsfc.nasa.gov.
- [9] E. A. Baltz *et al.*, *JCAP* **0807**, 013 (2008) [arXiv:0806.2911 [astro-ph]].
- [10] L. Bergstrom, J. Edsjo, P. Gondolo and P. Ullio, *Phys. Rev. D* **59**, 043506 (1999) [arXiv:astro-ph/9806072]; L. Bergstrom, J. Edsjo and P. Ullio, *Phys. Rev. D* **58**, 083507 (1998) [arXiv:astro-ph/9804050]; C. Calaneo-Roldan and B. Moore, *Phys. Rev. D* **62**, 123005 (2000) [arXiv:astro-ph/0010056]; A. Tasitsiomi, J. M. Siegal-Gaskins and A. V. Olinto, *New Astron. Rev.* **48**, 473 (2004) [arXiv:astro-ph/0306561]; A. Tasitsiomi and A. V. Olinto, *Phys. Rev. D* **66**, 083006 (2002) [arXiv:astro-ph/0206040]; F. Stoehr, S. D. M. White, V. Springel, G. Tormen and N. Yoshida, *Mon. Not. Roy. Astron. Soc.* **345**, 1313 (2003) [arXiv:astro-ph/0307026]; S. M. Koushiappas, A. R. Zentner and T. P. Walker, *Phys. Rev. D* **69**, 043501 (2004) [arXiv:astro-ph/0309464]; E. A. Baltz, J. E. Taylor and L. L. Wai, arXiv:astro-ph/0610731; L. Pieri, E. Branchini and S. Hofmann, *Phys. Rev. Lett.* **95**, 211301 (2005) [arXiv:astro-ph/0505356]; L. Pieri,

- G. Bertone and E. Branchini, arXiv:0706.2101 [astro-ph]; J. Diemand, M. Kuhlen and P. Madau, *Astrophys. J.* **657**, 262 (2007) [arXiv:astro-ph/0611370]; V. Berezhinsky, V. Dokuchaev and Y. Eroshenko, *JCAP* **0707**, 011 (2007) [arXiv:astro-ph/0612733]; V. Berezhinsky, V. Dokuchaev and Y. Eroshenko, *Phys. Rev. D* **68**, 103003 (2003) [arXiv:astro-ph/0301551]; L. E. Strigari, S. M. Koushiappas, J. S. Bullock and M. Kaplinghat, *Phys. Rev. D* **75**, 083526 (2007) [arXiv:astro-ph/0611925]; B. Moore, C. Calcaneo-Roldan, J. Stadel, T. Quinn, G. Lake, S. Ghigna and F. Governato, *Phys. Rev. D* **64**, 063508 (2001) [arXiv:astro-ph/0106271]; V. Springel *et al.*, arXiv:0809.0894 [astro-ph]; M. Kuhlen, J. Diemand and P. Madau, arXiv:0805.4416 [astro-ph]; S. Ando, *Phys. Rev. Lett.* **94**, 171303 (2005) [arXiv:astro-ph/0503006]; T. Oda, T. Totani and M. Nagashima, *Astrophys. J.* **633**, L65 (2005) [arXiv:astro-ph/0504096]; J. M. Siegal-Gaskins, V. Pavlidou, A. V. Olinto, C. Brown and B. D. Fields, *J. Phys. Conf. Ser.* **60**, 312 (2007) [arXiv:astro-ph/0611273].
- [11] S. Ando and E. Komatsu, *Phys. Rev. D* **73**, 023521 (2006) [arXiv:astro-ph/0512217]; S. Ando, E. Komatsu, T. Narumoto and T. Totani, *Phys. Rev. D* **75**, 063519 (2007) [arXiv:astro-ph/0612467].
- [12] A. Cuoco, S. Hannestad, T. Haugbolle, G. Miele, P. D. Serpico and H. Tu, *JCAP* **0704**, 013 (2007) [arXiv:astro-ph/0612559]; A. Cuoco, J. Brandbyge, S. Hannestad, T. Haugboelle and G. Miele, *Phys. Rev. D* **77**, 123518 (2008) [arXiv:0710.4136 [astro-ph]].
- [13] J. M. Siegal-Gaskins, arXiv:0807.1328 [astro-ph].
- [14] D. Hooper and P. D. Serpico, *JCAP* **0706**, 013 (2007) [arXiv:astro-ph/0702328].
- [15] S. M. Koushiappas, *Phys. Rev. Lett.* **97**, 191301 (2006) [arXiv:astro-ph/0606208]; S. Ando, M. Kamionkowski, S. K. Lee and S. M. Koushiappas, arXiv:0809.0886 [astro-ph].
- [16] T. D. Willis, arXiv:astro-ph/0201515.
- [17] coss.c.gsfc.nasa.gov/coss/egret.
- [18] J. F. Navarro, C. S. Frenk and S. D. M. White, *Astrophys. J.* **490**, 493 (1997) [arXiv:astro-ph/9611107].
- [19] A. R. Pullen, R. R. Chary and M. Kamionkowski, *Phys. Rev. D* **76**, 063006 (2007) [arXiv:astro-ph/0610295].
- [20] G. D. Mack, T. D. Jacques, J. F. Beacom, N. F. Bell and H. Yuksel, arXiv:0803.0157 [astro-ph].
- [21] P. A. G. Scheuer, *Proc. Cam. Phil. Soc.* **53**, 764 (1957).